

# **Systematics of 4f electron energies relative to host bands by resonant photoemission of rare earth ions in aluminum garnets**

C. W. Thiel, H. Cruguel,<sup>\*</sup> H. Wu,<sup>†</sup> Y. Sun, G. J. Lapeyre, and R. L. Cone  
*Department of Physics, Montana State University, Bozeman, MT 59717*

R. W. Equall  
*Scientific Materials Corporation, 310 Icepond Road, Bozeman, MT 59715*

R. M. Macfarlane  
*IBM Almaden Research Center, 650 Harry Road, San Jose, CA 95120*  
(February 9, 2001)

## **Abstract**

The energies of trivalent rare earth ions relative to the host valence band were measured for a series of rare-earth-doped yttrium aluminum garnets,  $R_xY_{3-x}Al_5O_{12}$  ( $R=Gd, Tb, Dy, Ho, Er, Tm, Yb, Lu$  and  $0 \leq x \leq 3$ ), using ultraviolet photoemission spectroscopy. The 4f photoemission spectra were acquired using synchrotron radiation, exploiting the 4d to 4f “giant resonance” in the 4f electron photoemission cross-section to separate the 4f contribution. Theoretical valence band and 4f photoemission spectra were fit to experimental results to accurately determine electron energies. The measured 4f<sup>n</sup> ground state energies of these ions range from 700 meV above the valence band maximum for  $Tb^{3+}$  to 4.7 eV below the valence band maximum for  $Lu^{3+}$ , and all ground state energies, except for  $Tb^{3+}$ , are degenerate with valence band states. An empirical model is successful in describing the relative energies of the 4f<sup>n</sup> ground states for rare earth ions in these materials. This model is used to estimate the positions of the lighter rare earth ions, giving good agreement with published excited state absorption and photoconductivity measurements on  $Ce^{3+}$  in yttrium aluminum garnet. It is shown that the energies of the 4f electrons relative to the valence band can be estimated from the photoemission spectrum of the undoped host, providing a simple method for extending these results to related host crystals. The success of this model suggests that further studies of additional host compounds will rapidly lead to a broader picture of the effect of the host lattice on the 4f electron binding energies.

## I. INTRODUCTION

There is a great body of work on the optical spectra of rare earth impurities in insulating host crystals, with the vast majority involving the atomic-like intraconfigurational  $4f^n$  to  $4f^n$  transitions. Due to the shielding provided by the outer closed shells of 5p and 5s electrons, the  $4f^n$  electronic states exhibit a strong atomic character that makes them of particular interest for both fundamental research and optical applications that benefit from their unique properties. In contrast to the extensive information available about the  $4f^n$  electronic states, much less is known regarding the relationships between localized  $4f^n$  levels and the electronic band states of the host crystal. Systematic study of the positions of  $4f^n$  levels relative to the host band states for rare earth ions in a range of materials is necessary to improve the understanding of interactions between these two very different types of electronic states and to allow models with predictive power to be developed and refined. With this goal in mind, we have studied a series of rare earth ions over a range of concentrations in yttrium aluminum garnet and applied an empirical model for purposes of explanation and prediction.

In this paper, we present the results of resonant photoemission spectroscopy on trivalent rare earth ions in yttrium aluminum garnet (YAG), the most important host crystal for rare earth solid-state lasers. Photoemission spectroscopy offers several advantages over other techniques and can provide information that complements optical measurements. Photoemission allows the energies of both valence and atomic (core) electronic states to be directly determined relative to a common energy reference, whereas interpretation of optical methods such as excited state absorption and photoconductivity may be complicated by uncertainty regarding the nature of the initial and final states involved. We employed resonant photoemission to measure the binding energies of the 4f and valence band electrons for the series of rare earth ions from  $Gd^{3+}$  through  $Lu^{3+}$ , which allowed the 4f and valence band spectra to be separated and analyzed independently by exploiting resonances in the 4f photoemission.<sup>1,2</sup> The photoemission spectra of both the valence band and 4f electrons were fit to theoretical models to provide accurate estimates for electron energies and relative positions. Since very little is known about the effect of concentration on the relative energies of the  $4f^n$  levels and band states, measurements were made for materials with rare earth concentrations ranging from pure YAG to the stoichiometric rare earth aluminum garnets. Our measurements indicate that the energies of both the rare earth ions and the valence band maximum (VBM)—the highest energy valence band state—are insensitive to the doping concentration to within an experimental accuracy of a few hundred meV.

The relative positions of different trivalent rare earth ions are successfully described by an empirical two-parameter model for the effect of the host crystal. For the heavier rare earth ions, it is shown that the relative energies are well described by the difference in free-ion ionization potentials. When extended to the lighter rare earth ions, which are significantly larger than yttrium, a correction for the change in ionic radius must be included to obtain accurate energies. This model is used to predict the binding energies of the lighter rare earth ions in YAG and the results agree well with published excited state absorption and photoconductivity measurements, indicating that measurements on as few as two different rare earth ions in a host are sufficient to predict

the energies of the remaining ions. A method derived from an electrostatic model for the effect of the host lattice is also suggested for estimating the binding energies of rare earth ions that substitute for yttrium through measurement of the binding energies of the yttrium core levels in either doped or undoped samples.

## II. BACKGROUND

Developing a complete picture of the electronic structure of rare-earth-doped insulators is essential for understanding interactions between rare earth ions and host band states and how they influence basic material properties. In particular, charge transfer between the rare earth ions and the host can lead to broad absorption bands in the visible or ultraviolet regions of the spectrum, possibly resulting in generation of color centers in the lattice. Because the charge transfer transition strength depends on the spatial overlap between the initial and final electronic states, intense metal-to-ligand charge transfer bands may appear in an ion's excited state absorption spectrum even when no corresponding feature is observed in the ground state absorption spectrum; this is particularly important when the excited state is a mixed configuration such as  $4f^{m-1}5d^1$ . Host band states may also influence the atomic transitions of the ion itself by inducing broadening and an increase in transition probability for forbidden transitions through hybridization, while interactions between the band states and the 4f electrons also provide a mechanism for energy transfer, non-radiative relaxation, and nonlinear optical effects. These processes are all of fundamental physical interest since they represent coupling between the two extremes of highly localized and strongly correlated 4f electrons of the rare earth ion and de-localized one-electron band states of the host crystal.

The rare earth ions have found numerous applications in modern technology as optically active impurity ions doped into both insulators and semiconductors. For many of these applications, knowledge of the position of the localized 4f electronic states relative to the band states of the crystalline host lattice is important for understanding the performance of an optical material. For example, in solid-state laser materials, charge transfer transitions from the excited states of rare earth ions to the conduction band of the host lattice often cause a parasitic absorption that overlaps lasing wavelengths, resulting in crystal heating, reduction of both gain and tuning range, and may completely inhibit laser action, as for  $Ce^{3+}$  and  $Pr^{3+}$  in yttrium aluminum garnet (YAG).<sup>3-5</sup> Excited state absorption can also create color centers and optical damage and is the dominant reason for the failure of otherwise promising tunable blue and ultraviolet laser materials.<sup>6,7</sup> In contrast, ionization can be beneficial for applications such as proposed optical memories, optical processors, and frequency standards based on photorefractive effects or photon-gated photoionization holeburning, which may employ controlled ionization of the rare earth ions for non-volatile data storage and processing.<sup>8</sup> The one- and two-photon photoionization process can potentially cause undesirable photodarkening of rare-earth-doped optical fibers and is a mechanism for the generation of optical gratings in these fibers.<sup>9</sup> The radiation hardness of optical materials, which is essential for space based applications, is strongly influenced by the energy of the rare earth ions relative to the host bands. In the particular case of YAG, some rare earth ions resist radiation damage, while others suffer damage through oxidation or reduction.<sup>10</sup> Recent studies suggest that the

efficiency of scintillator and phosphor materials is influenced by the position of the  $4f^n$  levels relative to the band states through both ionization of excited rare earth ions and energy exchange between band states and  $4f^n$  states.<sup>11,12</sup> In new luminescent materials for plasma and flat panel displays, the performance limitations of potential red and blue electroluminescent materials may arise from field-induced or thermal ionization of the rare earth ions.<sup>13</sup>

Most past experimental and theoretical work to locate  $4f^n$  energies relative to the crystal's electronic states has focused on metals and mixed valence materials, particularly cerium compounds;<sup>14,15</sup> however, there have also been notable efforts to characterize the  $4f^n$  energies of divalent and trivalent rare earth impurities in insulating host materials. X-ray photoemission spectra of the valence band and 4f electrons have been examined by Wertheim *et al.*<sup>16</sup> for the full series of rare earth trifluorides, where both the final state structure of the 4f photoemission and general trends in the 4f binding energies were noted. Much of the work on optical materials has involved optical measurements of transition energies using excited state absorption or photoconductivity and has arisen from the search for blue and ultraviolet laser materials based on the high-energy transitions of the divalent and trivalent rare earths.<sup>3-5,17,18</sup> The need for more efficient phosphor and scintillator materials has led to measurements of the position of the  $4f^n$  levels relative to band states in oxides containing  $Ce^{3+}$ ,  $Pr^{3+}$ ,  $Eu^{2+}$ ,  $Yb^{3+}$ , and  $Lu^{3+}$  as both impurities and host constituents.<sup>12,19</sup> Pedrini *et al.*<sup>20</sup> have also characterized the  $4f^n$  levels relative to band states by studying the photoionization thresholds of the divalent rare earth ions in several alkaline earth fluorides and comparing them to thresholds calculated from an electrostatic point-charge model.

### III. APPARATUS AND SAMPLES

The photoemission experiments were performed on the Iowa State/Montana State ERG/Seya beam line at the University of Wisconsin-Madison Synchrotron Radiation Center. The Aladdin electron storage ring was operated at 800 MeV or 1 GeV and the synchrotron radiation was dispersed with a combined ERG/Seya monochromator.<sup>21</sup> The extended range grasshopper (ERG) monochromator was used for these experiments and operated primarily in the energy range of 125 eV to 185 eV, with the resolution varying between 125 meV and 275 meV, respectively. The focused spot size at the sample position was 1 mm by 20  $\mu$ m for these experiments. The measurement end-station on the beam line consisted of three chambers. The air interlock allowed for introduction of a sample from atmosphere into the main analysis chamber without breaking its vacuum. The mid-chamber located between the air interlock and the main chamber was used to outgas the sample and holder before introduction into the main chamber. The main chamber featured a VSW HA50 angle-resolved hemispherical energy analyzer on a double-axis goniometer, a manipulator with three translational and three rotational degrees of freedom, a sample cleaver, a low-energy electron flood gun, an  $Ar^+$  sputtering gun, and a magnesium evaporator. The analyzer was operated with constant electron pass energy providing a resolution of 250 meV; thus, the total instrumental resolution varied between 275 meV and 375 meV for the photon energies used. The analyzer was aligned to collect electrons emitted normal to the sample surface to maximize the

photoemission sampling depth, and the photon beam was typically incident at  $\sim 30^\circ$  from the surface normal.

The materials studied in this work were rare-earth-doped yttrium aluminum garnets ( $R_xY_{3-x}Al_5O_{12}$ ), which belong to the cubic space group Ia3d (number 230).<sup>22</sup> Rare earth concentrations greater than 5% were required to clearly observe the 4f photoemission with the current experimental arrangement. Ions larger than  $Gd^{3+}$  could not be doped into YAG with sufficient concentration for this series of experiments due to the increasing mismatch of ionic radius with  $Y^{3+}$ , which limited the materials that could be studied to the heavier rare earth ions ( $Gd^{3+}$  to  $Lu^{3+}$ ). Measurements were made on undoped YAG and rare-earth-doped samples with atomic concentrations ranging from 7% ( $x = 0.21$ ) to the stoichiometric rare earth aluminum garnets ( $x = 3$ ). The single crystal GdAG, TbAG, DyAG, and HoAG samples were grown from flux by S. Mroczkowski at the Department of Applied Physics, Yale University. All other samples were single crystals grown at Scientific Materials Corporation (Bozeman, MT) using the Czochralski method.

Due to the surface sensitivity of the photoemission process, particularly in the 100 eV to 200 eV energy range,<sup>23</sup> surface purity was essential. To insure clean surfaces, all samples were fractured *in situ* using the sample cleaver while the vacuum in the chamber was maintained at  $10^{-9}$  Torr or better at all times. Since YAG has no cleavage planes, fracturing the sample resulted in surfaces with random orientations that were typically uneven across the crystal and of visibly rough texture. No attempt was made to orient the samples. The photon beam was focused onto the smoothest region of each surface to minimize potential depth of field effects. No observable surface contamination was present in any spectra, although a broadening of several meV per minute was observed, possibly due to development of deep differential charging in the sample or relaxation of the fractured surface. To maintain the best possible surface quality for all collected spectra, the samples were re-fractured whenever spectral broadening became apparent. Each new surface was oriented differently due to the unconstrained nature of the fracture; as a result, spectra were collected with several surface orientations for each sample. There was no observable dependence on orientation in the experimental spectra, and all results presented here represent an average over several orientations. Both argon ion sputtering and sample heating were tested as alternate preparation methods; however, we found that sputtering significantly broadened the spectral features, while heating tended to produce metallic features in the spectrum, presumably from a depletion of oxygen from the surface.

#### IV. SAMPLE CHARGING CONSIDERATIONS

The process of photoemission ejects electrons from the sample being studied and thus generates a positive charge in the sample. In metals and semiconductors, the conductivity of the sample is sufficient to compensate any removed charge and maintain the sample at a uniform potential. In insulators such as YAG, the resistance of the sample is large enough that a significant positive potential will develop in the region of photoemission. The induced voltage retards ejected photoelectrons, reducing their kinetic energy at the detector and producing an apparent increase in the measured binding

energies.<sup>24</sup> Non-uniform charging of the sample can also cause electrons originating from different regions of the sample to experience different retarding potentials. This differential charging effect produces an overall broadening in the observed spectrum and may cause peak shapes to become distorted.<sup>25</sup> Sample charging is highly dependent on crystal purity and experimental conditions, and combinations of electron flooding and spectral calibration to a reference peak are commonly used to compensate for its effects.<sup>26</sup>

For the YAG samples studied, photoemission resulting from the applied ultraviolet light rapidly generated a potential on the sample that was large enough to prevent observation of direct photoemission. To overcome this difficulty, an electron flood gun was used to partially compensate the positive charging from photoemission. We found that flooding electrons with low kinetic energy ( $\sim 10$  eV) minimized distortion and broadening of the spectral features. Residual charging shifts varied from a few eV to tens of eV for the different samples examined and were extremely sensitive to photon energy, surface orientation, and surface quality. Sequences of spectra were recorded independently to monitor time-dependent charging shifts and insure that there was no drift of the spectrum during the period of data acquisition. To further minimize the effect of time-dependent charging shifts, the maximum acquisition time was restricted to several minutes or less and the spectra were individually calibrated and then averaged together to obtain the final spectrum. The aluminum 2p photoemission peak was used as a reference for removal of relative charging shifts between different spectra of an individual sample. To check for shifts in the binding energy of Al 2p for different samples fractured *in situ*, magnesium was evaporated onto a fractured surface of each sample and the position of the Al 2p peak was measured relative to the metallic Mg 2p peak. The binding energy reference was established using the common method of placing the carbon 1s peak at a binding energy of 290 eV relative to the vacuum level (a value of 285 eV is often used when binding energies are referenced relative to the Fermi level of the analyzer).<sup>27,28</sup> The calibration was determined by measuring the positions of the core levels in pure YAG relative to the carbon 1s peak, and then using the Mg 2p and Al 2p peaks for subsequent binding energy calibrations. No carbon was observed on any samples fractured *in situ*; therefore, the binding energies were determined using the position of the small carbon 1s signal originating from adventitious carbon contamination on a YAG sample fractured in air. The measured binding energy of the center of the Al 2p peak was 78.8 eV for all samples studied, which agrees well with previous x-ray photoemission studies of core levels in YAG.<sup>29</sup> Since the precise binding energy of carbon 1s depends on the chemical environment (varying between 290 eV and 291 eV for hydrocarbon contaminants)<sup>27</sup> and contact potentials present in the electron analyzer, absolute binding energies determined by calibrating to carbon 1s may exhibit a systematic shift relative to their true values; however, any systematic shift in the binding energies does not affect measurements of relative binding energies.

Differential charging was a source of broadening in the spectra and arose from several sources such as the irregular nature of the fractured surfaces, inhomogeneity in the light intensity over the focused spot, reduced probability for electron escape for ions further from the surface, and electric fields originating from regions of the crystal not directly illuminated. The differential charging produced low binding energy tails on all of the spectral features as well as an overall broadening. A broadening that varied from

1.5 eV to 2.5 eV was observed in all spectra and was primarily attributed to differential charging, although lifetime broadening could also be a significant contribution.

In addition to simple broadening, spectral distortion due to differential charging was also observed in all spectra. The most obvious distortion was a double peaked structure present in the spectra of all samples for the photoemission peaks of both lattice constituents and metals evaporated onto the crystals. The double peaks had a relative shift that varied from 2 eV to 8 eV and an intensity ratio of roughly 1:5, with the weaker feature corresponding to regions of lesser charging. The same relative intensity and energy shift was observed for every photoemission peak in each spectrum, although the values could be significantly different for spectra taken at separate times. The relative intensity and energy shift observed in each spectrum was strongly dependent on all aspects of the experiment including sample alignment, electron gun current, source intensity, photon energy, and surface morphology. This effect was clearly due to differential charging and was attributed to a small transverse intensity variation over the source beam.

Since the charging distortion varied significantly between spectra, it was necessary to remove this effect from the data to permit the most accurate comparisons and consistent measurements. The observed peak shapes suggested modeling the measured spectra as resulting from simultaneous photoemission from two separate regions of the sample with different surface potentials. This model viewed the spectrum as composed of two spectra that were identical except for a relative shift, different intensities, and a relative change in broadening. A relative broadening was included to allow for variations in differential charging between the two regions of the sample, with the weaker feature typically broadened by a few hundred meV relative to the stronger feature. This model was sufficient to separate the two components present in the spectrum without making further assumptions regarding the actual shapes of the photoemission peaks. A nonlinear fitting routine was used on the relatively sharp Al 2p photoemission peak in each spectrum to determine the relative shift, intensity, and broadening of the two components in the model. This model produced excellent results for removal of the charging distortion, and the parameters determined from fitting the Al 2p peak were effective in describing the charging distortion for all features in each spectrum. Figure 1 shows an example of this process for 25% Yb:YAG. The distortion present in the valence band region is relatively small, but must be removed in order to make precise comparisons between spectra.

## V. ANALYSIS OF 4f AND VALENCE BAND PHOTOEMISSION SPECTRA

Photoemission spectroscopy measures the kinetic energy distribution of electrons ejected from a sample exposed to monochromatic light. These energy distribution curves may be used, together with knowledge of the photon energy, to infer the binding energy distribution of the electronic states in the sample. In addition to the features arising from the direct emission of electrons from the sample, a background due to inelastically scattered, or secondary, electrons is also present in the photoemission spectrum. This secondary electron background was removed from each individual photoemission peak when comparing and analyzing spectra. To subtract the background, the well-known

Shirley method was employed in which the magnitude of the secondary electron background at any kinetic energy is approximated as proportional to the total direct photoemission at higher kinetic energies.<sup>30</sup> This model was applied iteratively until the estimated background matched the actual background on both sides of the photoemission peak under consideration.

The photoemission spectrum contains information about both the 4f electrons of the rare earth impurity and the electronic states of the host crystal, allowing the energies of the states to be measured relative to a common reference. In section V A, we outline the use of resonant photoemission to identify and extract the 4f component of the crystal's photoemission spectrum. Sections V B and V C discuss the analysis of the structure of the 4f and valence band photoemission, respectively. In section V D, the binding energy measurements are summarized and discussed.

### A. Separating the 4f and valence band photoemission spectra

One of the difficulties in measuring the position of the 4f<sup>n</sup> levels using photoemission is that they often overlap the host valence band. To extract the 4f component of the spectrum, we employed the technique of resonant photoemission spectroscopy, which exploits resonances in the photoemission cross-section through the flexibility provided by synchrotron radiation.<sup>1</sup> For the partially filled 4f shell of rare earth ions, a “giant resonance” in the 4f photoemission occurs for photon energies that excite the atomic 4d<sup>10</sup>4f<sup>n</sup> to 4d<sup>9</sup>4f<sup>n+1</sup> transition of the ion.<sup>2,16,31</sup> This transition energy lies between 100 eV and 200 eV for the trivalent rare earth ions,<sup>32</sup> and the technique of constant initial-state-energy spectroscopy (CIS)<sup>33</sup> was used to locate the precise position and shape of this resonance for each rare earth ion studied in YAG. CIS measures the photoemission cross-section as a function of photon energy; thus, the 4f resonance can clearly be discerned in the CIS spectrum of the valence band region (~5 eV to ~20 eV binding energy) for photon energies from 100 eV to 200 eV. An example CIS spectrum for DyAG is displayed in Fig. 2, as well as photoemission spectra taken at four different photon energies ranging from the minimum of the 4f photoemission to the maximum. The shape of the resonance in the 4f photoemission shows a complex structure due to both the 4f level structure and coupling to the 4d hole, with the individual components exhibiting a distinctive Fano lineshape resulting from interference between the resonant 4d to 4f Auger component and direct 4f component of the photoemission.<sup>1,34</sup> This interference effect causes the total 4f photoemission to be initially suppressed and then enhanced as the photon energy is increased. Because of the relatively large change in the 4f photoemission cross-section over this region, the 4f component may be extracted by subtracting a spectrum taken at the minimum of the 4f photoemission from a spectrum taken at the maximum, scaled by a factor to compensate for the small change in the valence band cross-section,<sup>35</sup> as shown for 7% Gd:YAG in Fig. 3. The scaling factor, with typical values of 1.0 to 1.1, is necessary to insure that the valence band contributions in both spectra are equal and therefore cancel when taking the difference. The precise values of the scaling factors were determined by measuring the CIS spectra of both the valence band and Al 2p peak in undoped YAG and then using the measured photoemission intensity of the Al 2p peak in each spectrum to normalize for both the overall electron yield and changes in the valence band cross-section. Because the photon

energy dependence of the cross-section was determined from undoped YAG, any potential resonance in the valence band resulting from hybridization of the 4f electrons with the valence band were ignored; nevertheless, this effect should be small since mixing of the  $4f^n$  states with the valence band is expected to be negligible. Once the 4f spectrum was obtained, an estimate of the valence band spectrum was acquired by subtracting the small 4f component from the spectrum taken at the minimum of the 4f photoemission.

For  $\text{Lu}^{3+}$ , an alternate method was necessary to obtain the 4f spectrum since there is no 4d to 4f transition because of the filled 4f shell. The  $\text{Lu}^{3+}$  spectrum was extracted by using the different photon energy dependence of the photoemission cross-sections of the rare earth 4f electrons and valence band electrons, which are primarily of oxygen 2p character in YAG.<sup>36</sup> Over the energy range of 100 eV to 200 eV, the 4f cross-section remains nearly constant while the oxygen 2p cross-section rapidly decreases.<sup>37</sup> As a result, the  $\text{Lu}^{3+}$  spectrum may be obtained by subtracting a spectrum taken at low photon energy from a spectrum taken at high photon energy, scaled such that the valence band contributions are equal in both spectra.

Once the photon energies corresponding to the minimum and maximum of the 4f photoemission were determined, spectra were taken for several photon energies between these extremes and compared in a pair-wise manner to produce a series of 4f spectra. All generated 4f spectra were compared for consistency in both the removal of charging effects and compensation of the different valence band cross-sections. Final 4f spectra were generated for each sample by averaging the 4f spectra obtained from each pair of photon energies. Since any peculiarities in the spectra due to charging distortions or calibration errors were usually different for each spectrum, the averaging process tended to reduce distortions to a simple broadening that minimized the possibility of systematic errors. The 4f spectra for a representative concentration of each rare earth ion studied are given in Fig. 4, along with the spectrum of undoped YAG.

## B. Analysis of 4f photoemission final state structure

The 4f photoemission spectra show structure that extends over a range of up to 10 eV corresponding to excitation of upper electronic states of the tetravalent rare earth ions.<sup>38,39</sup> This structure arises because the photoemission process may leave the emitting ion in an excited state, reducing the kinetic energy of the ejected electron, and therefore resulting in an apparent increase in binding energy due to the final state of the system. The contribution to the photoemission spectrum from each final state can be described by the projections of the  $4f^n$  ground state wavefunction—with a single electron removed—onto the electronic states of the  $4f^{n-1}$  configuration; thus, the energy levels of the tetravalent ion each contribute to the observed photoemission to a varying degree. The relative magnitude of each level's contribution to the photoemission spectrum was estimated using the fractional parentage method described by Cox.<sup>40</sup> The relative energies of the components present in the photoemission final state structure are given by the energies of the  $4f^{n-1}$  levels of the tetravalent ion, which may be approximated by the well-known level structure of the isoelectronic trivalent ion,<sup>41</sup> expanded by 5% to 15% to account for the enhanced effective nuclear charge of the tetravalent ion.<sup>39</sup> This approximation of the tetravalent energy levels and their relative contributions to the

photoemission structure is sufficient for quantitative interpretation of the 4f photoemission spectra and determination of 4f binding energies.

The parameter of greatest interest for this study is the 4f ionization threshold—the energy required to remove one 4f electron and leave the remaining tetravalent rare earth ion in its ground state. Although the low binding energy edge of the 4f photoemission gives a rough estimate for the ionization threshold, broadening obscures the exact location, requiring a method for determining the binding energy of the ground state component of the final state structure to facilitate a quantitative analysis of the results. To obtain a precise measurement of the 4f ground state binding energy, the theoretical final state structure of the 4f photoemission, including spin-orbit splittings, was fit to the observed 4f photoemission. The fitting process adjusted the energy, intensity, and broadening of the theoretical final state structure to match the observed spectra. The energy scale factor due to the enhanced effective nuclear charge was also allowed to vary within the expected range of values during the fitting process since the exact values are not known. The fit of the theoretical final state structure to the observed 4f spectrum is displayed in Fig. 4 for each rare earth ion studied, where the dotted line is the fit and underlying tetravalent energy levels are shown as vertical lines. The height of each vertical line represents its relative contribution to the photoemission and only states that contribute at least 0.1% to the total intensity are shown. By matching the predicted spectra to the measured spectra, particularly for the low binding energy region of the 4f photoemission, the binding energy that corresponds to leaving the tetravalent ion in its ground state was estimated and compared to the energy of the VBM. The agreement between the predicted structure and data is not perfect due to approximations in the calculation of the final state structure, residual valence band contributions, and distortion from differential charging. Using more accurate wavefunctions in the calculations of the final state structure would also improve the agreement, particularly for terbium,<sup>39</sup> however, this description of the final state structure is adequate to determine the energy of the ground state component with an estimated accuracy of several hundred meV. For most samples, the 4f spectra appeared to exhibit an additional broadening of 0.5 eV to 1.5 eV relative to the broadening of the valence band and core levels, possibly due to changes in differential charging and calibration between the different spectra used to generate the 4f spectra or lifetime broadening of the 4f photoemission.

### C. Analysis of valence band photoemission

Since we are interested in measuring the energies of the 4f electrons relative to the band states, as well as the effects of the rare earth doping on the host lattice, an estimate for the binding energy of the VBM is required for each material studied. The photoemission spectrum of undoped YAG is plotted in Fig. 5, with the charging effects and secondary background removed. The VBM corresponds to the low binding energy edge of the valence band but experimental broadening obscures the exact location, making a precise measurement difficult. To overcome this difficulty, the observed valence band photoemission was compared to theoretical calculations. The theoretical shape of the valence band photoemission was estimated from the atom-resolved partial density of states calculations of Xu and Ching<sup>36</sup> weighted by the calculated atomic photoemission cross-sections from Yeh and Lindau.<sup>37</sup> The theoretical cross-section

broadened by 1.8 eV gave excellent agreement with the experimental data, allowing an estimate for the underlying VBM to be obtained. Using this method, a value of 8.7 eV was determined for the binding energy of the VBM. A similar procedure was performed to determine the position of the VBM for each sample studied.

No significant dependence on crystal orientation was observed in the spectra, and the measured results represent an average over several random crystal orientations. This result is expected since the top of the valence band in YAG is very flat, with maximum variations of less than a few hundred meV throughout the Brillouin zone.<sup>36</sup> A flat valence band is characteristic of yttrium and aluminum oxides and implies that the relative energy of the VBM and  $4f^n$  states has very little orientation dependence in this class of materials.

#### D. Results of measurements and analysis

The measured binding energies of the  $4f^n$  ground states are given in Table I for all samples studied. Since the VBM exhibited a constant binding energy for all samples to within the experimental accuracy, and energy differences are unaffected by errors in absolute calibration, the position of the  $4f^n$  ground states are referenced relative to the VBM binding energy of 8.7 eV. Of the ions studied,  $Tb^{3+}$ , which was 700 meV above the VBM, was the only ion with its  $4f^n$  ground state energy within the host band gap. The  $4f^n$  ground states of all other ions studied were degenerate with valence band states, with  $Lu^{3+}$  having the lowest ground state energy at 4.7 eV below the VBM.

To study the effects of concentration on the energy level structure of the samples, rare earth concentrations varying between pure YAG and the stoichiometric rare earth aluminum garnets were examined. Although information about the valence band could be obtained from all samples, the limitations of the experimental arrangement prohibited extraction of useful 4f spectra for samples with concentrations lower than 5%. A comparison of the 4f spectra of each ion for different concentrations revealed that, while the photoemission intensity was roughly proportional to the concentration as expected, the 4f binding energies were unchanged within the experimental accuracy of several hundred meV for the full range of concentrations studied. Additional comparisons of measurements on erbium-doped yttrium aluminum garnet and erbium-doped lutetium aluminum garnet did not reveal any significant shift in the  $Er^{3+}$  binding energy. This may also be viewed as a lack of concentration dependence where the yttrium has been replaced by lutetium rather than the particular rare earth ion being studied.

The results discussed above indicate that binding energies obtained for one concentration may be used as an estimate for all concentrations, to within the current experimental accuracy of several hundred meV. Further measurements are required to determine whether there are observable concentration shifts in other materials, with effects more likely to be observed for materials where the rare earths substitute for ions with a significantly different radius or materials in which the rare earth ions compose a large fraction of the host volume.

Except for slight changes in the overall shape, the valence band remained essentially unchanged by the addition of rare earth ions, and the valence band maximum maintained a constant binding energy within the experimental accuracy. The dominant oxygen 2p character of the electronic states comprising the valence band, particularly in

the low binding energy region, might explain the limited effect of the rare earth ion concentration.<sup>36</sup> In contrast, the strong yttrium and rare earth character of the low-energy conduction band states might predict a dependence on both rare earth ion and concentration for the band gaps of the materials.

## VI. SYSTEMATIC BEHAVIOR OF THE 4f BINDING ENERGIES

There are several approaches to modeling the binding energies of localized electronic levels in a crystalline environment such as density-functional theory,<sup>42</sup> the renormalized atom approach,<sup>43</sup> thermodynamic arguments,<sup>44</sup> and electrostatic methods.<sup>28</sup> One model applicable to localized levels in an ionic host lattice is the electrostatic point-charge model, which was first applied to the estimation of ionization thresholds by Pauling.<sup>45</sup> Various versions of this model have since been used to predict the relative binding energies of core levels, absolute binding energies of electrons, excited state absorption energies, and photoionization thresholds.<sup>18–20,46</sup> The essence of this model is to consider the lattice as consisting of point charges with integer valence, and then to calculate the shift in binding energy resulting from the electrostatic interactions between the ion and host. In this picture, we view the free-ion electron binding energy—which by definition is measured relative to the vacuum level—as being shifted by the electrostatic potential, or Madelung potential, of the lattice site that the ion occupies. Other effects that must be considered in these calculations include (in order of decreasing importance) polarizability of the lattice, distortion of the lattice site due to the presence of the impurity, inter-atomic Born repulsive energies, and Van der Waal’s forces. These terms are generally of significant magnitude compared to the total binding energy, with the final result arising through partial cancellation of relatively large energies with opposite signs, requiring that all effects be calculated precisely. Because of this complexity, calculations of absolute binding energies based on this method are generally of limited accuracy and difficult to extend to more than a few materials because of the amount of information needed for accurate calculations.

### A. Shift of the ionization potential

Regardless of the accuracy in predicting *absolute* binding energies, one significant consequence of an electrostatic model is that the *differences* in binding energies for different ions should be approximately equal regardless of the host material. These binding energy differences are most easily found from differences of the known trivalent rare earth free-ion ionization potentials,<sup>47</sup> which correspond to 4f electron binding energies in the free-ions. The shielded nature of the 4f electrons in the trivalent rare earth ions should provide an ideal case for application of this model, whereas, for most ions, this is an oversimplification due to the electronic mixing with the lattice (covalency) and the changes in the ionic and electronic radii. To test this approximation, we have compared the differences in published values of the free-ion ionization potentials to the measured 4f binding energies in YAG. This is shown in Fig. 6, where our measurements are represented by circles on the plot and the shifted free-ion ionization potentials correspond to the dotted line. The uniform binding energy shift was

determined by shifting the average of the free-ion ionization potentials to the average of the measured binding energies, resulting in a shift of 31.6 eV. This simple model gives reasonable agreement with the experimental data to within the combined error bars of the published values for the ionization potentials and the experimental error in determining the binding energies. Due to the phenomenological nature of this model, it has the potential to describe effects not incorporated in an electrostatic model.

The agreement between the simple electrostatic model and the measured binding energies suggests several methods for estimating the 4f electron binding energies for a series of ions from a single measurement. For example, measurements for one rare earth ion in a material should give an estimate for the energies of all the rare earth ions by considering the differences in the free-ion ionization potentials. Since this method relies on the similarity in ionic radii, the accuracy of the estimate would decrease for larger changes in the ionic radius. For materials in which the rare earth ion substitutes for yttrium, which has an ionic radius similar to the rare earths, the electrostatic model suggests the possibility of estimating rare earth binding energies from the shift in the yttrium ion binding energies. This method would use the intrinsic yttrium ion in a host crystal as a “probe” for determining the effective electrostatic interactions at the lattice site, and then use this information to predict the effect of the lattice on the binding energies of a rare earth ion placed at that site. For trivalent yttrium, the least bound electrons belong to the filled 4p shell, with a free-ion ionization potential of 61.8 eV.<sup>48</sup> The photoemission spectrum of the yttrium 4p electrons shows the final state structure due to the spin-orbit splitting of the  $J=3/2$  and  $J=1/2$  levels, where the splitting is 1.2 eV and the  $J=3/2$  level is the ground state of the ionized yttrium.<sup>49</sup> Thus, in a manner similar to the method used for rare earth ions, the electron energy that corresponds to leaving the tetravalent yttrium ion in its ground state may be determined by measuring the position of the  $4p_{3/2}$  level from the photoemission spectrum. In oxides, the oxygen 2s peak lies a few eV below the yttrium 4p peaks, requiring that the oxygen and yttrium peaks be fit simultaneously. The measured position of the  $4p_{3/2}$  level is 30.4 eV in YAG, giving a shift of 31.4 eV relative to the free-ion value, which agrees well with the 31.6 eV shift measured from the rare earth ions. In the simplest approximation, the binding energy shift should be uniform for all core levels, allowing an estimate to be obtained from the shift of one of the well-resolved core levels. For example, the measured  $3d_{5/2}$  peak in YAG is at 162.5 eV, and should be  $\sim 132.7$  eV from  $4p_{3/2}$ ,<sup>49</sup> giving a shift of 32.0 eV. This agreement suggests that analysis of the undoped host’s photoemission spectrum may be sufficient to predict the 4f electron energies of the rare earth ions with an ionic radius similar to yttrium’s.

## B. Effect of ionic radius

The electrostatic model may also be used to extrapolate our observed binding energies in YAG to the lighter rare earth ions, but the effect of the change in ionic radius must be included in the model to obtain accurate estimates for ions with a radius significantly different from yttrium. This effect arises primarily from the distortion of the lattice site caused by the presence of the rare earth ion and was first considered by Pedrini *et al.*<sup>18</sup> for the case of divalent rare earth ions in the fluorides, where it was found to be important for describing the observed 4f photoionization thresholds. Any change in the

ionic radius affects all of the terms in the electrostatic model through the corresponding changes in bond lengths; as a result, theoretical calculations of this effect would require precise knowledge of the lattice distortions induced by the presence of the impurity ion. Fortunately, the change in ionic radius across the rare earths is small enough to allow the net effect to be modeled as linear in ionic radius. This approximation allows the proportionality constant to be treated as an empirical parameter that can be determined from measurements on two different ions, with comparison of  $\text{Ce}^{3+}$  and  $\text{Lu}^{3+}$  giving the best estimate. Since this approach to the electrostatic model only contains two unknown parameters, measurements on two different rare earth ions in an ionic host should be sufficient to predict the positions of all the remaining ions in that host, even when substituting for ions with a significantly different radius.

Using the two-parameter model, we extrapolated our measurements for YAG to the lighter rare earth ions as shown in Fig. 6. This empirical model is given by the following equation:  $E_{4f} = I - E_L + \alpha_R(R - R_0) - E_{VBM}$ , where  $E_{4f}$  is the 4f binding energy relative to the VBM,  $I$  is the free-ion ionization potential,  $E_L$  is the intrinsic electrostatic effect of the lattice ( $E_L = 31.6$  eV),  $\alpha_R$  is the binding energy shift per unit change in ionic radius,  $R$  and  $R_0$  are the effective ionic radii of the trivalent rare earth and yttrium ions in eight-fold co-ordination ( $R_0 = 1.019$  Å),<sup>50</sup> and  $E_{VBM}$  is the binding energy of the valence band maximum ( $E_{VBM} = 8.7$  eV). The dotted line in Fig. 6 corresponds to this model with a constant binding energy shift ( $\alpha_R = 0$ ), and the solid line corresponds to the full model ( $\alpha_R \neq 0$ ). The error bars in Fig. 6 represent the uncertainty in the free-ion ionization potentials for the ions studied, while the error bars on the extrapolated values for  $\text{Eu}^{3+}$  through  $\text{Ce}^{3+}$  also include the uncertainty in the extrapolation due to the accuracy of the two fit parameters. The effect of the ionic radius was determined by fitting our data to the linear model for the deviation from the free-ion ionization potentials, weighted by the accuracy of the free-ion ionization potentials used in the model. The resulting fit to our measurements indicates an  $\alpha_R = 8.3$  eV/Å effect in YAG arising from the change in ionic radius. This causes the estimated binding energy of  $\text{Ce}^{3+}$  to be increased by 1.0 eV and the estimated binding energy of  $\text{Lu}^{3+}$  to be reduced by 0.35 eV. The origin of this shift can be understood in terms of the effect on the ion's nearest neighbors. An increase in ionic radius increases the distance to the negatively charged neighbors, therefore reducing the negative electrostatic potential at the rare earth site and increasing the energy required to remove a 4f electron, while the opposite is true for a decrease in radius. A change in radius affects the polarization and repulsive energies as well as the electrostatic potential, but the change in lattice potential should be the dominant contribution to the observed shifts.

It is important to note that although the electrostatic point-charge model provided the motivation for describing the 4f binding energies with a two-parameter model, the limitations of the electrostatic model do not necessarily apply to the empirical model. An empirical treatment avoids weaknesses of the electrostatic point-charge model, such as failure to consider covalency in the lattice, details of the charge distribution, and modifications of the atomic contributions to the binding energy. The two-parameter model allows the effects of these processes to be incorporated into the empirical constants even though they cannot be adequately treated within the theoretical framework of a purely electrostatic model. The success of this empirical picture of the rare earth binding energies is derived from the well-known chemical similarity of the rare earth ions

and their similar response to the host lattice. Thus, we expect that the empirical two-parameter model will have much wider applicability than a purely electrostatic model, allowing extension to a wide range of materials, possibly including materials with significant covalency such as semiconductors.

### C. Comparison with optical measurements and extension to related hosts

Excited state absorption and photoconductivity measurements on Ce:YAG and Pr:YAG allow comparisons to be made with the extrapolation of our measurements using the empirical two-parameter model. Estimates for the energies of  $\text{Ce}^{3+}$  and  $\text{Pr}^{3+}$  relative to the VBM from these published results are included in Fig. 6. Given that both of these techniques involve transitions to the conduction band of the host, knowledge of the band gap is necessary to determine the energies relative to the VBM. The photoconductivity measurements of Pedrini *et al.*<sup>20</sup> on Ce:YAG show that  $\text{Ce}^{3+}$  is 3.8 eV below the conduction band; thus, since the band gap of YAG is 6.5 eV,<sup>51</sup> this places the  $4f^n$  ground state at 2.7 eV above the VBM, which agrees with the value of  $2.4 \text{ eV} \pm 0.3 \text{ eV}$  extrapolated from our measurements. Excited state absorption measurements have been made on both  $\text{Ce}^{3+}$  and  $\text{Pr}^{3+}$  in YAG, although in both cases the absorption thresholds occurred below the measured energy ranges, requiring that the position of the rare earth ion relative to the conduction band be estimated by extrapolating the low energy absorption signal back to its onset. In Ce:YAG, Hamilton *et al.*<sup>4</sup> estimated that  $\text{Ce}^{3+}$  was 2.5 eV above the VBM, which is in good agreement with both the photoconductivity measurements and our estimate. Although there has been some uncertainty as to whether the observed excited state absorption and photoconductivity signals in Ce:YAG corresponded to direct transitions to the conduction band or to higher rare earth configurations, such as  $4f^{n-1}6p^1$ , the agreement between the estimated thresholds and the energies extrapolated from our photoemission measurements supports the conclusion that the final state is indeed the conduction band.<sup>7</sup> For Pr:YAG, Cheung and Gayen<sup>5</sup> proposed that  $\text{Pr}^{3+}$  was 1.2 eV above the VBM, which is larger than our estimate of  $0.4 \text{ eV} \pm 0.3 \text{ eV}$ . This discrepancy could be attributed to the combined errors in the measurements; however, it may also indicate either that the excited state absorption threshold in Pr:YAG is due to the upper  $4f^{n-1}5d^1$  levels or crystal defects rather than the conduction band or that the  $\text{Pr}^{3+}$  ionization potential used in our model is too large. Further measurements on  $\text{Pr}^{3+}$  doped materials can be used to provide a quantitative analysis of the model's predictions for  $\text{Pr}^{3+}$  and the consequences for Pr:YAG.

The 4f binding energy of  $\text{Eu}^{3+}$  relative to the VBM in europium gallium garnet (EuGG) as determined from photoemission measurements is also included in Fig. 6 for comparison.<sup>52</sup> Although the binding energies will be shifted relative to YAG, the effects on the VBM and 4f binding energies are expected to be relatively small due to the similar structure of the materials. Since the largest effect on the electrostatic potential should arise from nearest-neighbor ions, we may make a rough estimate for the energy shift of the 4f binding energy by comparing the change in bond lengths between the two materials with the observed effect of ionic radius in YAG. The increase in average yttrium-oxygen bond length in YGG compared to YAG is half of the change in bond length between YAG and GdAG.<sup>53</sup> Given that the estimated shift between YAG and GdAG due to the change in bond length is less than 300 meV to higher binding energy

(using  $\alpha_R=8.3$  eV/Å), we estimate that the 4f binding energy in EuGG might only be 100 meV to 200 meV larger than in EuAG. The effect on the VBM is more difficult to estimate, but is probably at most a few hundred meV. The measured value of  $\sim 3.4$  eV below the VBM in EuGG is shifted to higher binding energy as expected but is still within the uncertainty of the predicted value of  $2.8 \text{ eV} \pm 0.6 \text{ eV}$  in EuAG, implying that the difference in relative binding energies between the two crystals is at most several hundred meV.

The extrapolation of our photoemission results using the empirical model offers an opportunity to consider implications for the important solid-state laser material Nd:YAG. The predicted energy of the  $\text{Nd}^{3+}$  ground state is 900 meV below the VBM in YAG, which places the  $4f^n$  ground state at 7.4 eV below the bottom of the conduction band. This shows that the single-photon absorption threshold from the  $\text{Nd}^{3+}$  ground state to the host conduction band is expected to occur at an energy significantly higher than the fundamental absorption of YAG. Ionization of the  $\text{Nd}^{3+}$  through a multi-photon process involving 1.064  $\mu\text{m}$  photons would require a very low probability five-photon absorption from the upper laser level, and even the high-energy photons of a flashlamp pump source would lack sufficient energy to ionize a 4f electron. Thus, the large 4f binding energy of  $\text{Nd}^{3+}$  in YAG clearly contributes to the well-known efficiency and resistance to optical damage exhibited by high-power Nd:YAG laser systems. Since the measured binding energy of the  $4f^n$  ground state of  $\text{Yb}^{3+}$  is even larger than for  $\text{Nd}^{3+}$ , ionization would be even less likely to occur in high-power Yb:YAG laser systems.

The success of these comparisons suggests that further studies of additional host compounds will rapidly lead to a clearer picture for the effect of the host lattice on the 4f electron binding energies. That broad picture of the electronic structure of rare-earth-doped optical materials will motivate fundamental theoretical analysis and will be directly useful for designing new optical materials.

## VII. CONCLUSION

Photoemission spectroscopy is a useful tool for locating the energy of localized rare earth impurity levels relative to host band structure in optical materials. In particular, the ability to measure energies of electronic states relative to a common reference avoids many of the difficulties in interpretation that are present in optical methods and provides information that complements excited state absorption and photoconductivity measurements. Using synchrotron radiation, resonances in the 4f photoemission cross-section, such as the 4d to 4f “giant resonance”, may be exploited to uniquely identify the 4f component of a photoemission spectrum from the often-overlapping host valence band. The ability to separate the 4f spectrum from the host spectrum allows the relative binding energies of the valence band maximum and 4f electrons to be determined. This energy separation is a material parameter that is important for many technological applications of optical materials, such as solid-state lasers, phosphors, scintillators, electroluminescent devices, rare-earth-doped optical fibers, optical memories, and optical processors.

To explore the systematics of the binding energies of the rare earth  $4f^n$  electronic states relative to the host valence band, we have performed resonant photoemission

spectroscopy on a series of rare earth ions doped into yttrium aluminum garnet. The binding energies of the 4f ground state and the valence band maximum were measured for rare earth ions from  $\text{Gd}^{3+}$  to  $\text{Lu}^{3+}$  at atomic concentrations varying from 7% to 100%. No concentration dependence of the 4f or the VBM binding energies was observed, suggesting that measurements for a single concentration are sufficient to locate the binding energies for samples of any concentration; however, we might expect a noticeable effect on the conduction band, which is primarily formed from cation electronic states in an ionic host. To test this, a series of experiments using a technique complementary to photoemission, such as inverse photoemission or photoconductivity, will be required.

To explain the relative binding energies of the different rare earth ions, we employed an empirical model for the effect of the host lattice on the ion's binding energy. This model describes the differences in binding energies of the rare earth ions as due to differences in free-ion ionization potentials, modified by a smaller effect due to the variation in ionic radii. Fitting the measured binding energies gave good agreement, with a 31.6 eV shift of the free-ion ionization potentials and an additional 8.3 eV/Å effect arising from the difference of the rare earth and yttrium ionic radii. This model was supported by further comparison with energies obtained from published photoconductivity and excited state absorption measurements. The empirical model's success in describing the systematic trends in 4f binding energies indicates that measurements on two rare earth ions in the host may be sufficient to predict the energies of all other rare earth ions in that host, particularly if the accuracies of the free-ion ionization potentials used in the model are improved by further comparison with measurements.

Another consequence of this model is that, when rare earth ions substitute for ions of similar radius, it may be possible to obtain preliminary estimates of the rare earth binding energies through measurement of the binding energy shift of the host crystal's intrinsic ions. This method is motivated by the ionic nature of the rare earth bonding in insulating optical materials and allows the rare earth energies to be estimated from examination of the photoemission spectrum of the undoped host crystal, providing a quick and simple technique for surveying potential rare-earth-doped materials.

Additional data with more accurate measurements of electron binding energies will permit a detailed analysis of the empirical two-parameter model and test the range of materials for which it is applicable. Development of improved methods for charge compensation and reducing differential charging while insuring maximum uniformity in the photon beam intensity will improve the accuracy and sensitivity of the photoemission measurements. By comparing measurements in different materials with the empirical model, improved estimates for the free-ion ionization potentials may be obtained and used in the model to increase the accuracy of its predictions. Study of new materials will undoubtedly reveal lattice dependent trends that will enhance the predictive power of the empirical model.

Much work is still needed to advance the understanding of relationships between localized 4f electrons and the crystal band states. Measurements over the entire rare earth series in many different host materials are required to build a more complete picture of rare-earth-doped optical materials. Comparison of experimental results with theoretical predictions will provide insight into the electronic structure of the crystal lattice and

provide guidance for calculations of lattice dependent properties. By supplementing photoemission with complementary techniques such as photoconductivity, excited state absorption, bremsstrahlung isochromat spectroscopy, and inverse photoemission, the relationships and interactions between rare earth ions and the occupied and unoccupied electronic states of the host crystal may be thoroughly explored. With sufficient data to guide the theoretical treatment of these processes, it may become possible to better understand the properties of current optical materials as well as direct the development of new materials for specific applications.

### **ACKNOWLEDGMENTS**

The authors wish to thank C. G. Olson for advice regarding experimental techniques and apparatus. Samples for this project were supplied by Scientific Materials Corporation, Bozeman MT, and Stanley Mroczkowski and W. P. Wolf at the Applied Physics Department, Yale University. Funding for this research was provided in part by the Air Force Office of Scientific Research under Grant Nos. F49620-97-1-0411, F49620-98-1-0171, and F49620-00-1-0314. This material is based upon work supported under a National Science Foundation Graduate Research Fellowship. This work is based upon research conducted at the Synchrotron Radiation Center, University of Wisconsin-Madison, which is supported by the NSF under Award No. DMR-0084402.

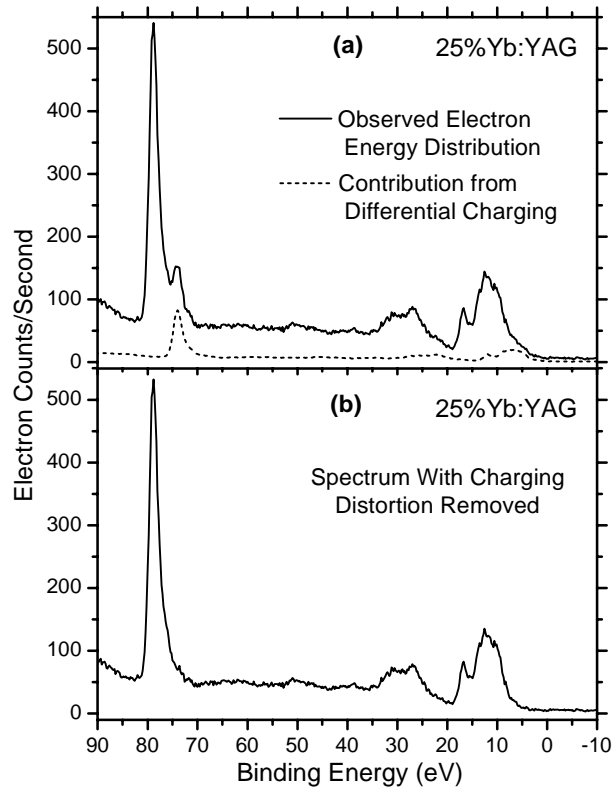
**FIGURES**FIG. 1. Thiel *et. al.*

Figure 1. Example of photoemission spectrum before and after removal of charging distortion (see Section IV). a) The solid line shows the photoemission spectrum of 25% Yb:YAG ( $h\nu=181.5$  eV) which is composed of two components with a relative charging shift, and the dotted line is the estimate of the smaller component of the spectrum as determined from fitting. b) The difference of the two spectra in the upper plot. The model used to determine the shape of the subtracted spectrum forces the two components to be identical except for a relative shift, different intensities, and a relative broadening. For this example, the weaker component (dotted line in a) corresponds to the stronger component (b) shifted by 4.8 eV, scaled by 0.16, and broadened by 100 meV.

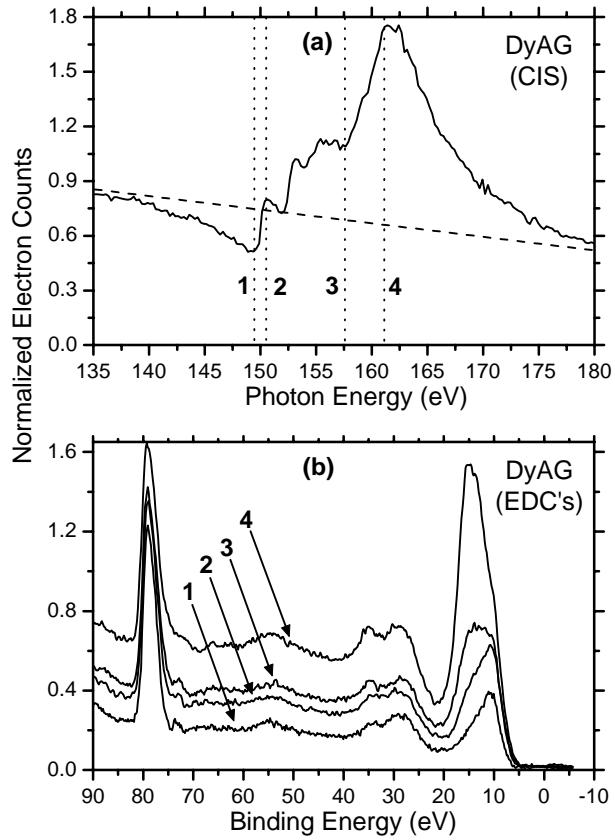
FIG. 2. Thiel *et. al.*

Figure 2. The 4d to 4f resonance in the 4f photoemission of DyAG. a) The constant-initial-state energy spectrum (CIS) of the valence band region (5 eV to 20 eV binding energy) of DyAG showing the 4d to 4f resonance in the 4f photoemission. The dashed line shows the trend of the combined valence band and 4f cross-section outside of the resonance. The four dotted vertical lines indicate the photon energies used in generating the 4f spectra ( $h\nu_1=149.5$  eV,  $h\nu_2=150.5$  eV,  $h\nu_3=157.5$  eV, and  $h\nu_4=161.0$  eV). b) The energy distribution curves (EDC's) corresponding to the four photon energies indicated in the CIS spectrum. The photoemission spectra have all been normalized to the intensity of the Al 2p peak and the charging effects have been removed as discussed in section IV.

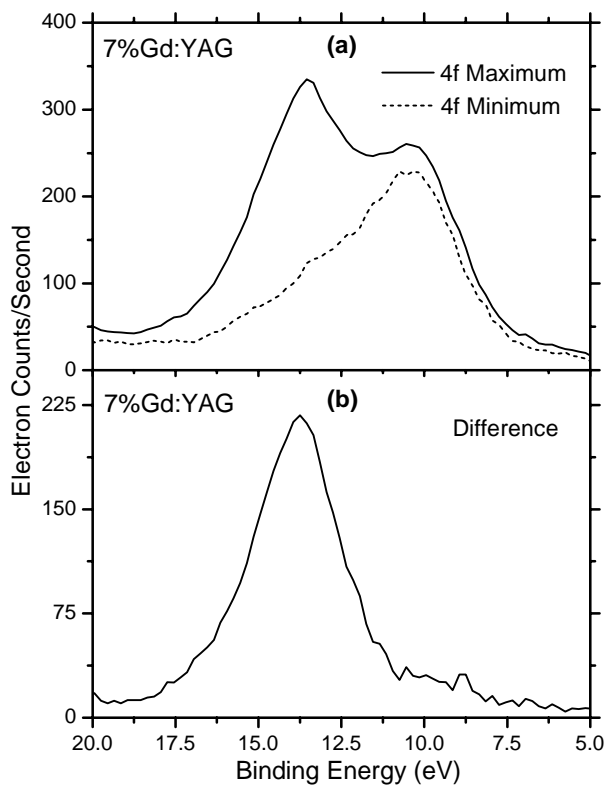
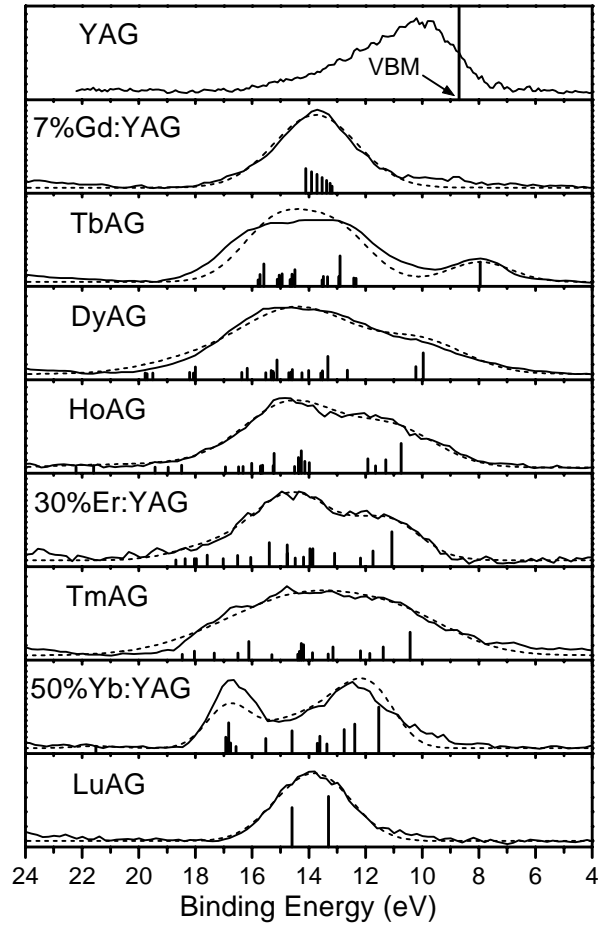
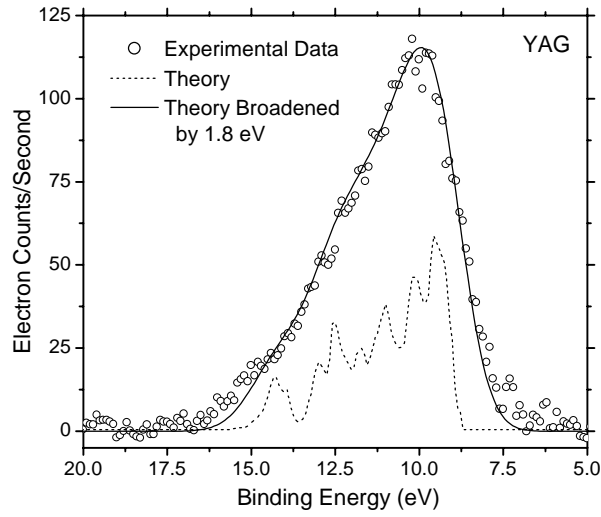
FIG. 3. Thiel *et. al.*

Figure 3. Example of extracting the 4f component of the photoemission spectrum. a) Spectra taken at the minimum ( $h\nu=144.0$  eV) and maximum ( $h\nu=148.5$  eV) of the 4f photoemission for 7%Gd:YAG. The spectra have been scaled so that the valence band component has the same amplitude in both spectra. b) The difference of the two curves in (a) gives the  $Gd^{3+}$  4f photoemission.



**FIG. 4.** Thiel *et. al.*

Figure 4. Representative data for each ion studied. Solid lines represent measured 4f photoemission spectra with the secondary electron background subtracted and dotted lines are fits to the theoretical final state structure (see section V). The vertical lines represent the underlying energy level structure and their height represents their relative contribution to the photoemission (only states that contribute more than 0.1% are shown). The valence band of YAG has been plotted for reference, with the position of the valence band maximum shown as a vertical line.



**FIG. 5.** Thiel *et. al.*

**Figure 5.** Circles represent the measured photoemission spectrum of undoped YAG ( $h\nu=125.0$  eV) with the secondary electron background subtracted. The dotted line is proportional to the theoretical valence band photoemission cross-section at this photon energy obtained using the results of Refs. 36 and 37. The solid line is the theoretical shape broadened by 1.8 eV and scaled to match the experimental data. By comparing the theoretical curve to the data, an estimate of 8.7 eV is obtained for the binding energy of the valence band maximum.

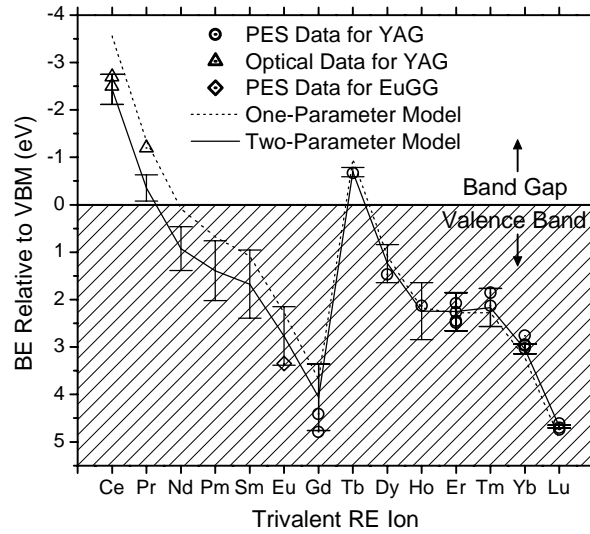


FIG. 6. Thiel *et. al.*

Figure 6. Systematic behavior of 4f binding energies relative to the valence band maximum. Circles represent our measured binding energies relative to the VBM (at 8.7 eV); negative binding energies are within the band gap of the host and positive energies are below the VBM. The dotted line is the fit of the empirical model to our measured values without considering the effect of ionic radius. The solid line is the fit of the model to our measured values including the effect of ionic radius. The error bars on the model are due to uncertainty in the values of the free-ion ionization potentials and the error bars on the extrapolated values for  $\text{Eu}^{3+}$  through  $\text{Ce}^{3+}$  include the uncertainty due to the accuracy of the fitting parameters. The triangles represent estimated positions from excited state absorption and photoconductivity measurements in Refs. 4, 5, and 20. The diamond is the estimated position in EuGG from Ref. 52. Note that the bottom of the conduction band lies at about  $-6.5$  eV.

**TABLES**

Table I. Measured 4f electron ground state binding energies relative to the valence band maximum for all samples studied. Following the usual sign convention for binding energies, positive values lie below the valence band maximum and negative values lie within the band gap.

<i>Dopant Ion</i>	<i>Concentration</i>	<i><math>\Delta BE</math> (eV)</i>
Gd	7%	4.8
Gd	100%	4.4
Tb	100%	-0.7
Dy	100%	1.5
Ho	100%	2.1
Er	30%	2.5
Er <sup>a</sup>	30%	2.3
Er	50%	2.5
Er	100%	2.1
Tm	10%	2.1
Tm	100%	1.9
Yb	10%	2.8
Yb	25%	3.0
Yb	50%	3.0
Yb	100%	3.0
Lu	50%	4.7
Lu <sup>a</sup>	70%	4.7
Lu	100%	4.6

<sup>a</sup>Measured in 30% erbium doped lutetium aluminum garnet.

## REFERENCES

\*Present address: Département de Recherche sur l'Etat Condensé, CEA/Saclay, F-91191 Gif-sur-Yvette Cedex, France

†Present address: Department of Physics, The University of Hong Kong, Pokfulam Road, Hong Kong, China

- <sup>1</sup> J. W. Allen, in *Synchrotron Radiation Research: Advances in Surface and Interface Science*, edited by R. Z. Bachrach (Plenum Press, New York, 1992), Vol. 1, pp. 253—323.
- <sup>2</sup> W. Lenth, F. Lutz, J. Barth, G. Kalkoffen, and C. Kunz, *Phys. Rev. Lett.* **41**, 1185 (1978); J. W. Allen, L. I. Johansson, R. S. Bauer, I. Lindau, and S. B. Hagström, *Phys. Rev. Lett.* **41**, 1499 (1978); W. Gudat, S. F. Alvarado, and M. Campagna, *Solid State Commun.* **28**, 943 (1978); B. Johansson, J. W. Allen, T. Gustafsson, I. Lindau, and S. B. Hagström, *Solid State Commun.* **28**, 53 (1978).
- <sup>3</sup> J. F. Owen, P. B. Dorain, and T. Kobayasi, *J. Appl. Phys.* **52**, 1216 (1981).
- <sup>4</sup> D. S. Hamilton, S. K. Gayen, G. J. Pogatshnik, R. D. Ghen, and W. J. Miniscalco, *Phys. Rev. B* **39**, 8807 (1989).
- <sup>5</sup> Y. M. Cheung and S. K. Gayen, *Phys. Rev. B* **49**, 14827 (1994).
- <sup>6</sup> R. R. Jacobs, W. F. Krupke, and M. J. Weber, *Appl. Phys. Lett.* **33**, 410 (1978).
- <sup>7</sup> K.-S. Lim and D. S. Hamilton, *J. Opt. Soc. Am. B* **6**, 1401 (1989).
- <sup>8</sup> R. M. Macfarlane and R. M. Shelby, in *Spectroscopy of Solids Containing Rare Earth Ions*, edited by A. A. Kaplyanski and R. M. Macfarlane (North Holland, Amsterdam, 1987), pp. 51—184; R. M. Macfarlane and G. Wittmann, *Opt. Lett.* **21**, 1289 (1996); G. Wittmann and R. M. Macfarlane, *Opt. Lett.* **21**, 426 (1996).
- <sup>9</sup> M. M. Broer, R. L. Cone, and J. R. Simpson, *Opt. Lett.* **16**, 1391 (1991); G. R. Atkins and A. L. G. Carter, *Opt. Lett.* **19**, 874 (1994).
- <sup>10</sup> S. Kh. Batygov, Yu. K. Voron'ko, B. I. Denker, A. A. Maier, V. V. Osiko, V. S. Radyukhin, and M. I. Timoshechkin, *Fiz. Tverd. Tela (Leningrad)* **14**, 977 (1972) [*Sov. Phys. Solid State* **14**, 839 (1972)].
- <sup>11</sup> G. Blasse and B. C. Grabmeier, *Luminescent Materials* (Springer, Berlin, 1994).
- <sup>12</sup> C. Dujardin, C. Pedrini, J. C. Gâcon, A. G. Petrosyan, A. N. Belsky, and A. N. Vasil'ev, *J. Phys.: Condens. Matter* **9**, 5229 (1997); U. Happek, S. A. Basun, J. Choi, J. K. Krebs, and M. Raukas, *J. Alloys Comp.* **303-304**, 198 (2000).
- <sup>13</sup> M. Ando and Y. A. Ono, *J. Appl. Phys.* **69**, 7225 (1991); K. Swiatek, M. Godlewski, L. Niinistö, and M. Leskelä, *J. Appl. Phys.* **74**, 3442 (1993).
- <sup>14</sup> M. Campagna, G. K. Wertheim, and Y. Baer, in *Topics in Applied Physics*, edited by L. Ley and M. Cardona (Springer-Verlag, Berlin, Heidelberg, 1979), Vol. 27, Chap. 4, p. 217—260.
- <sup>15</sup> D. W. Lynch and J. Weaver, in *Handbook on the Physics and Chemistry of Rare Earths*, edited by K. A. Gschneider, LeRoy Eyring, and S. Hufner (North-Holland, Amsterdam, 1987), Vol. 10, Chap. 66, p. 231.
- <sup>16</sup> G. K. Wertheim, A. Rosencwaig, R. L. Cohen, and H. J. Guggenheim, *Phys. Rev. Lett.* **27**, 505 (1971).
- <sup>17</sup> C. Pedrini, D. S. McClure, and C. H. Anderson, *J. Chem. Phys.* **70**, 4959 (1979).
- <sup>18</sup> J. K. Lawson and S. A. Payne, *Phys. Rev. B* **47**, 14003 (1993).
- <sup>19</sup> M. Raukas, S. A. Basun, W. van Schaik, W. M. Yen, and U. Happek, *Appl. Phys. Lett.* **69**, 3300 (1996); W. M. Yen, M. Raukas, S. A. Basun, W. van Schaik, and U. Happek, *J. Lumin.* **69**, 287 (1996).
- <sup>20</sup> C. Pedrini, F. Rogemond, and D. S. McClure, *J. Appl. Phys.* **59**, 1196 (1986).
- <sup>21</sup> C. G. Olson, *Nucl. Instrum. Methods Phys. Res. A* **266**, 205 (1988).
- <sup>22</sup> S. Geller, *Z. Kristallogr.* **125**, 1 (1967).
- <sup>23</sup> C. R. Brundle, *J. Vac. Sci. Technol.* **11**, 212 (1974).
- <sup>24</sup> R. T. Lewis and M. A. Kelly, *J. Electron Spectrosc. Relat. Phenom.* **20**, 105 (1980).
- <sup>25</sup> T. L. Barr, *J. Vac. Sci. Technol. A* **7**, 1677 (1989).
- <sup>26</sup> T. L. Barr, *J. Vac. Sci. Technol. A* **13**, 1239 (1995); J. B. Metson, *Surf. Interface Anal.* **27**, 1069 (1999).
- <sup>27</sup> T. D. Thomas, *J. Chem. Phys.* **52**, 1373 (1970).
- <sup>28</sup> C. K. Jørgensen, *Struc. Bonding* **24**, 1 (1975).
- <sup>29</sup> D. A. Pawlak, K. Woźniak, Z. Frukacz, T. L. Barr, D. Fiorentino, and S. Seal, *J. Phys. Chem. B* **103**, 1454 (1999).
- <sup>30</sup> D. A. Shirley, *Phys. Rev. B* **5**, 4709 (1972); P. M. A. Sherwood, in *Practical Surface Analysis*, edited by D. Briggs and M. P. Seah (Wiley, New York, 1983), pp. 445—475.

- <sup>31</sup> O. Gunnarsson and T. C. Li, Phys. Rev. B **36**, 9488 (1987).
- <sup>32</sup> C. G. Olson and D. W. Lynch, J. Opt. Soc. Am. **72**, 88 (1982).
- <sup>33</sup> G. J. Lapeyre, A. D. Baer, J. Hermanson, J. Anderson, J. A. Knapp, and P. L. Gobby, Solid State Commun. **15**, 1601 (1974); G. J. Lapeyre, Nucl. Instrum. Methods Phys. Res. A **347**, 17 (1994).
- <sup>34</sup> W. Gudat, S. F. Alvarado, M. Campagna, and Y. Pétrouff, J. Phys. (Paris), Colloq. **5**, 1 (1980).
- <sup>35</sup> J.-S. Kang, J. H. Hong, J. I. Jeong, S. D. Choi, C. J. Yang, Y. P. Lee, C. G. Olson, B. I. Min, and J. W. Allen, Phys. Rev. B **46**, 15689 (1992).
- <sup>36</sup> Y.-N. Xu and W. Y. Ching, Phys. Rev. B **59**, 10530 (1999).
- <sup>37</sup> J. J. Yeh and I. Lindau, At. Data Nucl. Data Tables **32**, 1 (1985).
- <sup>38</sup> P. A. Cox, Y. Baer, and C. K. Jørgensen, Chem. Phys. Lett. **22**, 433 (1973); E. I. Zabolotskii, Y. P. Irkhin, and L. D. Finkel'shtein, Fiz. Tverd. Tela (Leningrad) **16**, 1142 (1974) [Sov. Phys. Solid State **16**, 733 (1974)].
- <sup>39</sup> J. K. Lang, Y. Baer, and P. A. Cox, J. Phys. F **11**, 121 (1981).
- <sup>40</sup> P. A. Cox, Struc. Bonding **24**, 59 (1975).
- <sup>41</sup> G. H. Dieke and H. M. Crosswhite, Appl. Opt. **2**, 675 (1963); R. T. Wegh, A. Meijerink, R.-J. Lamminmäki, and J. Hölsä, J. Lumin. **87-89**, 1002 (2000).
- <sup>42</sup> W. Y. Ching, Y.-N. Xu, and B. K. Briceen, Appl. Phys. Lett. **74**, 3755 (1999).
- <sup>43</sup> J. F. Herbst, N. D. Lowy, and R. E. Watson, Phys. Rev. B **6**, 1913 (1972).
- <sup>44</sup> B. Johansson, J. Phys. F **4**, L169 (1974).
- <sup>45</sup> L. Pauling, Phys. Rev. **34**, 954 (1929).
- <sup>46</sup> C. S. Fadley, S. B. M. Hagström, M. P. Klein, and D. A. Shirley, J. Chem. Phys. **48**, 3779 (1968); P. H. Citrin and T. D. Thomas, J. Chem. Phys. **57**, 4446 (1972).
- <sup>47</sup> W. C. Martin, R. Zalubas, and L. Hagan, Natl. Stand. Ref. Data Ser. (U.S., Natl. Bur. Stand.) **60**, 1 (1978).
- <sup>48</sup> C. E. Moore, Natl. Stand. Ref. Data Ser. (U.S., Natl. Bur. Stand.) **34**, 1 (1970).
- <sup>49</sup> M. Cardona and L. Ley, in *Topics in Applied Physics*, edited by M. Cardona and L. Ley (Springer-Verlag, Berlin, Heidelberg, 1978), Vol. 26, p. 269.
- <sup>50</sup> R. D. Shannon, Acta Crystallogr. Sect. A **32**, 751 (1976).
- <sup>51</sup> G. A. Slack, D. W. Oliver, R. M. Chrenko, and S. Roberts, Phys. Rev. **177**, 1308 (1969).
- <sup>52</sup> C. W. Thiel, H. Cruguel, Y. Sun, G. J. Lapeyre, and R. L. Cone (unpublished).
- <sup>53</sup> F. Euler and J. A. Bruce, Acta. Cryst. **19**, 971 (1965).